Journal of Mines, Metals and Fuels, *71(12C) : 286-296; 2023. DOI: 10.18311/jmmf/2023/47285*

Print ISSN : 0022-2755

Journal of Mines, Metals and Fuels

Contents available at: *www.informaticsjournals.com/index.php/jmmf*

Effect of Viscous Dissipation and Thermal Radiation on Thermal Properties of MHD Nanofluid in a Curved Channel

C. Kavitha[1], Gullapalli Neeraja[2], M. S. Gayathri[3] and Sudhir Patel[4]

[1]Deptartment of Mathematics, GFGC Yelahanka, Bengaluru – 560064, Karnataka, India
[2]Deptartment of Mathematics, M S Ramaiah Institute of Technology, Bengaluru - 560 054, Karnataka, India; neeraja.g@msrit.edu
[3]Department of Mathematics, BMS College of Engineering, Bangalore - 560 019, Karnataka, India; msgayathri.math@bmsce.ac.in
[4]Department of Mathematics, New Horizon College of Engineering, Bangalore - 560 036, Karnataka, India; sudhirfriends@gmail.com

Abstract

The effects of radiation and magnetohydrodynamics on the peristaltic flow of a nanofluid through a porous media in a two-dimensional circular asymmetric channel have been theoretically analysed in terms of viscous dissipation. Under the assumption of a radially uniform magnetic field, the nanofluid is electrically conducting. The radiation response, thermophoresis, and Brownian motion are all taken into consideration by the transport equation. The assumptions of a long wavelength and a low Reynolds number have further simplified the problem. The impact of many parameters on the flow characteristics has been examined through graphical representations using MATLAB bvp4c. Further, impact of Nusselt and Sherwood numbers are studied and its effects are displayed through graphs. Also impact of Schmidt and Soret numbers are examined.

Keywords: Magnetic Field, Peristalsis, Schmidt and Soret Effect

1.0 Introduction

Peristalsis is an involuntary process of fluid movement in the form of progressive wave along a flexible channel. Peristalsis play the role of propelling and mixing fluid against pressure. It plays numerous roles in physiology. For example, movement of food through oesophagus, bowels down the anus, urine from kidney to bladder *etc*. Even in industries the process of peristalsis is used in roller pumps. Roller pumps are used to pump various fluids avoiding contamination and to carry slurries and highly reactive hazardous fluids. Among the advantages they provide are CIP and forward and reverse pumping directions to aid in the upstream piping and instrumentation cleaning process. It pushes the fluids against pressure rise and causes broad propulsive and mixing actions. Peristalsis helps in mineral enrichment using mineral processing reagents. It helps in reduced usage of water and chemical, lowering environmental risk. Peristalsis is also used in 3D printing. Peristaltic pump uses flexible tube which is squeezed by rollers. This provides consistent flow, giving quality prints.

**Author for correspondence*

Nanofluid is a fluid with suspension of nanoparticles. The fluid into which the suspension is added is known as base fluid. When compared to base fluids like water or oil, nanofluids have been found to have improved thermophysical properties like viscosity, thermal diffusivity, thermal conductivity, and convective heat transfer coefficients.

Casson nanofluids is a type of nanofluid which uses Newtonian fluid like water or oil as base fluid. It is a shear-thinning fluid exhibiting viscoelastic behaviour. It acts as a solid up to a specific shear stress. When an external force is applied, the soft solids start to flow. The minimal stress that initiates the flow is called yield stress. A non-Newtonian Casson fluid has yield stress as one of its characteristics. When the applied yield stress happens to be less than the shear stress, it is seen that fluid behaves like a solid and viscosity decreases as shear rate increases. Due to the existence of haemoglobin, blood is an appropriate bio magnetic fluid. Hence peristaltic flow is impacted by magnetic force. Ali *et al*., examined how heating affects viscous fluid transport in curved channel[1]. In comparison to a straight channel, they discovered that heat transmission decreases gradually in the curved course. Heat transport through an asymmetric channel under peristalsis of nanofluids were studied using the HPM by A.M. Abd-Alla *et al.,*[2]. Research has been done on how radiation and MHD affect a nanofluid's peristaltic flow along a porous medium in two-dimensional asymmetric channel, which is tappered by M. Kothandapani *et al*[3]., A.M. Abd-Alla *et al*., Akbar *et al.,* studied the MHD peristaltic flow of a Carreau nanofluid in an asymmetric channel[4]. It was discovered that when the thermophoresis parameter and Hartmann number increase, so does the pressure rise. Bhargava and Singh examined heat transfer flow of a second-grade fluid, taking into account joule heating and viscous dissipation[5]. B. Venkateswarlu *et al*., did a numerical investigation into this study inspect the consequences of heat source and viscosity dissipation on MHD flow and heat transmission from a warm, electrically conducting fluid to a melting surface in a consistent free stream[6]. O.D. Makinde *et al*., investigated the impact of velocity slip on heat transfer via an asymmetric channel fluid filled with a porous material and hydromagnetic flow of Casson fluid under peristalsis[7]. Mohammad M. Rashidi *et al.,* examined the heat and mass transfer analysis of the peristaltic wave-induced MHD blood flow in the Casson fluid model[8]. The impact of Joule heating and MHD on the peristaltic blood flow of an Eyring-Powell nanofluid in an irregular channel was investigated by Asha *et al*., Saba *et al*., examined the effects of heat transport and the simultaneous application of magnetic and electric fields on the peristaltic flow of a viscous fluid along a curved channel[9-11].

Recently many developments have taken place in the field of EOR (Enhanced Oil Recovery) using nanofluids. Work of Hu *et al*., showed that there is remarkable increase in EOR[12]. Shear thinning nanofluid can increase the viscosity of displacing fluid, which helps in removing drilling mud. Nanoparticles can manoeuvre its way through porous rocks and interact with large oil molecules so that it is disintegrated into droplets, as shown by Zhang *et al*. and Suleimanov *et al.,*[13,14]. Moghadam *et al*., showed that ZnO nanoparticles helps in reducing IFT (Interfacial Tension) between crude oil and injected fluid[15]. After secondary flooding, electromagnetic nanofluids can assist in additional oil recovery. This was proposed by Adil *et al*.,[16] by lowering pipeline friction, Casson nanofluids can increase the refinery's capability to transport fluids, including crude oil. These nanofluids can be effectively transferred along pipes using peristalsis pumps[17]. Peristalsis is often used in mining operations to move slurry. Casson nanofluids can be used to improve the slurry's viscosity and flow properties. By employing peristaltic pumps, slurry can be transferred efficiently from one location to another[18].

This paper aims to investigate flow of Casson nanofluid in an asymmetric channel which is nonuniform, caused by sinusoidal peristaltic waves. The effect of viscous dissipation and thermal radiation on has received little attention. The goal of this study is to investigate the combined effects of Hall and viscous dissipation on the peristalsis of an electrically conducting Casson nanofluid in a curved channel, driven by the previously mentioned facts. Radiative heat flux and flexible walls are also taken into account. The long wavelength and low Reynolds number assumptions simplify the governing equations. MATLAB is used to compute the solutions to the reduced equations. With the aid of graphs, the impact of relevant parameters on physical quantities of interest are demonstrated and thoroughly discussed.

Paper examines the effect of joule heating and MHD on peristaltic blood flow of a Eyring–Powell nanofluid in a non-uniform channel.

Here we analysed the effect of joule heating on peri-staltic blood flow of Eyring–Powell nanofluid in a non-uniform channel, is modelled in the presence of MHD

2.0 Mathematical Formulation

We examine the Casson nanofluid flow within a porous curved channel, coiled around O as its centre. The radius is taken to be R. Let 2a be the width of the channel (Figure 1). $\bar{V}$ is the velocity of the flow produced by peristalsis. The mathematical depiction of flow patterns in the laboratory frame is done using the curvilinear coordinate system $(\bar{r}, X, t)$, where wall temperature and concentration are denoted by T_0, C_0, and T_1, C_1 for the upper and lower walls, respectively. $\bar{r}$ is along radial direction and X being parallel to the flow direction. Let V be the radial component of $\bar{V}$ and U be its axial component.

Upper and lower walls are given by

$$H(X,t) = \pm a \pm b\sin\left(\frac{2\pi}{\lambda}(X - ct)\right) \tag{1}$$

where b, λ, c, H are amplitude, wavelength, wave speed and radial displacement of walls. It is assumed that wavelength is large when compared to width of the channel,

i.e., $\frac{a}{\lambda} \le 1$.

For Casson fluid model, stress tensor is given by

$$\tau_{ij} = \begin{cases} 2\left(\mu + \frac{p_y}{\sqrt{2\pi}}\right)e_{ij}, & if\ \pi > \pi_c \\ 2\left(\mu + \frac{p_y}{\sqrt{2\pi_c}}\right)e_{ij}, & if\ \pi < \pi_c \end{cases} \tag{2}$$

Here $\pi = e_{ij}e_{ij}$ where e_{ij} is the (i, j) th component of deformation rate, $\mu, p_y\ and\ \pi_c$ are plastic dynamic viscosity, yield stress and critical value respectively.

We have $p_y = \frac{\mu\sqrt{2\pi_c}}{\beta}$, where β is Casson material parameter, μ is fluid viscosity (3)

The magnetic field along radial direction is $B = \left[\frac{RB_0}{\bar{r}+R}, 0, 0\right]$ where B_0 is strength of magnetic field (4)

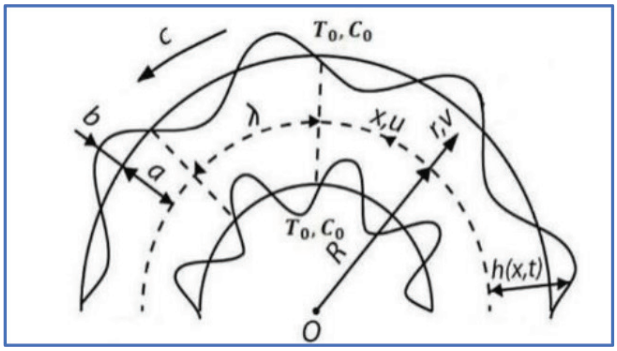


Figure 1. Wave in curved channel.

The current density J is given by $J = \sigma(V \times B)$, where σ is electric conductivity of nanofluid

$$= \left[0, 0, \frac{-\sigma R B_0 U}{\bar{r}+R}\right] \tag{5}$$

Lorentz force F, which is a combination of electric and magnetic force, is

$$F = J \times B$$

$$= \left[0, -\frac{\sigma R^2 B_0{}^2 U}{(\bar{r}+R)^2}, 0\right] \tag{6}$$

Equations governing for the flow are

$$\frac{\partial(\bar{r}+R)V}{\partial\bar{r}} + R\frac{\partial U}{\partial X} = 0 \tag{7}$$

$$\rho\left[\frac{\partial V}{\partial t} + (\bar{V}\cdot\nabla)V - \frac{U^2}{\bar{r}+R}\right] = -\frac{\partial P}{\partial\bar{r}} + \mu\left(1+\frac{1}{\beta}\right)\left[\nabla^2 V - \frac{V}{(\bar{r}+R)^2} - \frac{2R}{(\bar{r}+R)^2}\frac{\partial U}{\partial X}\right] \tag{8}$$

$$\rho\left[\frac{\partial U}{\partial t} + (\bar{V}.\nabla)U + \frac{UV}{\bar{r}+R}\right] = -\frac{R}{\bar{r}+R}\frac{\partial P}{\partial X} + \mu\left(1+\frac{1}{\beta}\right)\left[\nabla^2 U - \frac{U}{(\bar{r}+R)^2} + \frac{2R}{(\bar{r}+R)^2}\frac{\partial V}{\partial X}\right] + -\frac{\sigma R^2 B_0{}^2 U}{(\bar{r}+R)^2} - \rho g\beta_T(T-T_0) - \rho g\beta_C(C-C_0) \tag{9}$$

$$(\rho c)_p\left[\frac{\partial T}{\partial t}+\left(\overline{V}\cdot\nabla\right)T\right]=k\nabla^2T+\frac{\sigma R^2B_0{}^2U^2}{\left(\overline{r}+R\right)^2}+\frac{\partial q_{\overline{r}}}{\partial\overline{r}}$$
$$+\mu\left[2\left(\frac{\partial V}{\partial\overline{r}}\right)^2+\left(\frac{R}{\overline{r}+R}\frac{\partial V}{\partial X}-\frac{U}{\overline{r}+R}\right)\right.$$
$$\left.\left(\frac{\partial U}{\partial\overline{r}}+\frac{R}{\overline{r}+R}\frac{\partial V}{\partial X}-\frac{U}{\overline{r}+R}\right)+\frac{\partial U}{\partial\overline{r}}\left(\begin{array}{c}\frac{\partial U}{\partial\overline{r}}+\frac{R}{\overline{r}+R}\\ \frac{\partial V}{\partial X}-\frac{U}{\overline{r}+R}\end{array}\right)\right]$$
$$+2\left(\frac{R}{\overline{r}+R}\frac{\partial U}{\partial X}+\frac{V}{\overline{r}+R}\right) \quad (10)$$

$$\frac{\partial C}{\partial t}+\left(\overline{V}\cdot\nabla\right)C=D\nabla^2C+\frac{DK_T}{T_m}\nabla^2T \quad (11)$$

Where $\overline{V}.\nabla=V\frac{\partial}{\partial\overline{r}}+\frac{RU}{\overline{r}+R}\frac{\partial}{\partial X}$ (12)

$$\nabla^2=\frac{\partial^2}{\partial\overline{r}^2}+\frac{1}{\overline{r}+R}\frac{\partial}{\partial\overline{r}}+\left(\frac{R}{\overline{r}+R}\right)^2\frac{\partial^2}{\partial X^2} \quad (13)$$

and $q_{\overline{r}}$ is radiative heat flux and

$$q_{\overline{r}}=\frac{-16\sigma T_0^3}{3k^*}\frac{\partial T}{\partial\overline{r}} \quad (14)$$

In the above equations $\rho, g, \beta_T, \beta_C, k, c_p, D, K_T, T_m$ are fluid density, acceleration due to gravity, coefficient of thermal expansion heat, coefficient of expansion with concentration, thermal conductivity, specific heat, mass diffusivity coefficient, thermal diffusivity coefficient, mean temperature.

The following transformations are employed to shift laboratory frame $(\overline{r}, X)$ to wave frame (r, x),

$$\begin{aligned}&x=X-ct, r=\overline{r}, p(r,x)=P(\overline{r},X,t), v=V,\\&u=U-c, T=T, v(r,x)=V(\overline{r},X,t),\\&u(r,x)=U(\overline{r},X,t), \sigma(r,x)\\&=\sigma(\overline{r},X,t), \theta(r,x)=\theta(\overline{r},X,t)\end{aligned} \quad (15)$$

Introducing non-dimensional variables

$$x'=\frac{x}{\lambda}, r'=\frac{r}{a}, u'=\frac{u}{c}, v'=\frac{v}{\delta c}, \delta=\frac{a}{\lambda}, t'$$
$$=\frac{ct}{\lambda}, \phi=\frac{b}{a}, k'=\frac{R}{a}, p'=\frac{a^2p}{\mu c\lambda}, \sigma=\frac{C-C_1}{C_0-C_1},$$

$$\theta=\frac{T-T_0}{T_1-T_0}, M^2=\frac{a^2B_0{}^2\sigma}{\mu}, G_r=\frac{\rho g\beta_T\left(T_1-T_0\right)a^2}{\mu c},$$
$$G_c=\frac{\rho g\beta_C\left(C_1-C_0\right)a^2}{\mu c}, R_n=\frac{16\sigma\left(T_1-T_0\right)^3}{3k^*k},$$
$$P_r=\frac{\mu c_p}{k}, E_c=\frac{c^2}{c_p\left(T_1-T_0\right)}, Br=\frac{\mu c^2}{k\left(T_0-T_1\right)}$$
$$=Ec.\Pr, R_e=\frac{\rho ca}{\mu}, S_c=\frac{\upsilon}{D}, S_r=\frac{DK_T\left(T_1-T_0\right)}{\nu T_m\left(C_1-C_0\right)}, \quad (16)$$

Where $M, G_r, G_c, R_n, P_r, E_c, B_r, R_e, S_c, S_r, k^*$ are Hartmann number, thermal Grashoff number, concentration Grashoff number, Radiation parameter, Prandtl number, Eckart number, Brinkmann number, Reynolds number, Schmidt number, Soret number, mean absorption coefficient.

The stream function ψ is defined by $u=\frac{-\partial\psi}{\partial r}$ and

$$v=\frac{k}{r+k}\frac{\partial\psi}{\partial x} \quad (17)$$

Applying (15), (16) and (17), assuming low Reynolds number and long wavelength, in equations (7) to (11)), removing hash, reduces to

$$\frac{\partial p}{\partial r}=0 \quad (18)$$

$$-A\left(r+k\right)\frac{\partial^4\psi}{\partial r^4}-2A\frac{\partial^3\psi}{\partial r^3}+\frac{A+B}{\left(r+k\right)}\frac{\partial^2\psi}{\partial r^2}$$
$$-\frac{\left(A+B\right)}{\left(r+k\right)^2}\frac{\partial\psi}{\partial r}+\frac{\left(A+B\right)}{\left(r+k\right)^2}-G_r(r+k)\frac{\partial\theta}{\partial r}+ \quad (19)$$
$$-G_c(r+k)\frac{\partial\sigma}{\partial r}-G_r\theta-G_c\sigma=0$$

$$\left[\left(1-R_n\right)\frac{\partial^2\theta}{\partial r^2}+\frac{1}{r+k}\frac{\partial\theta}{\partial r}\right]+B_r\left(\frac{\partial\psi}{\partial r}\right)^2+B_r\left(1+B\right) \quad (20)$$
$$\left(\frac{1}{r+k}\right)^2\left(\frac{-\partial\psi}{\partial r}+1\right)^2+-\frac{2B_r}{r+k}\left(\frac{-\partial\psi}{\partial r}+1\right)=0$$

$$\frac{1}{S_c}\left[\frac{1}{r+k}\frac{\partial\sigma}{\partial r}+\frac{\partial^2\sigma}{\partial r^2}\right] +S_r\left[\frac{1}{r+k}\frac{\partial\theta}{\partial r}+\frac{\partial^2\theta}{\partial r^2}\right]=0 \quad (21)$$

where $A=1+\frac{1}{\beta}$, $B=M^2k^2$

The boundary conditions which are non-dimensional are

$$\psi=F,u=0,\theta=1,\sigma=1,at\ r=h$$
$$\psi=-F,u=0,\theta=0,\sigma=0,at\ r=-h \quad (22)$$

3.0 Result and Discussions

Since equations (24) to (26) are highly non-linear, MATLAB bvp4c is utilised in order to solve the system with boundary conditions (27) and plot. Impact of Casson parameter β, Hartmann number M, curvature K, thermal Grashoff number G_r, concentration Grashoff number G_c, radiation parameter R_n, Brinkmann number B_r, Soret number S_r, Schmidt number S_c on velocity, temperature, concentration, pressure variation along the direction of flow and pressure rise per wavelength would be studied.

3.1 Velocity Profile

The Casson nanofluid display shear-thinning characteristic. As the Casson parameter β increases yield stress increases. Hence extra force is required to initiate and sustain the fluid flow. As Casson parameter β increases resistance to flow increases. Hence velocity decreases, which can be observed in Figure 2(a). Velocity is increasing as curvature K is increasing, observable in Figure 2(b). As K increases fluid is exposed to centrifugal force. This promotes increase in velocity, especially where curvature is more pronounced. Also, fluid travels faster over a curved channel so that it covers same distance in same time. Hartmann number M is the ratio of Lorentz force to the viscosity. The Lorentz force produced by the applied magnetic field gets stronger as M raise. This force acts as retarding force acting perpendicular to the direction of the current flow and the magnetic field. This causes velocity to decrease. This can be observed in Figure 2(c). Thermal Grashoff number Gr is the ratio of

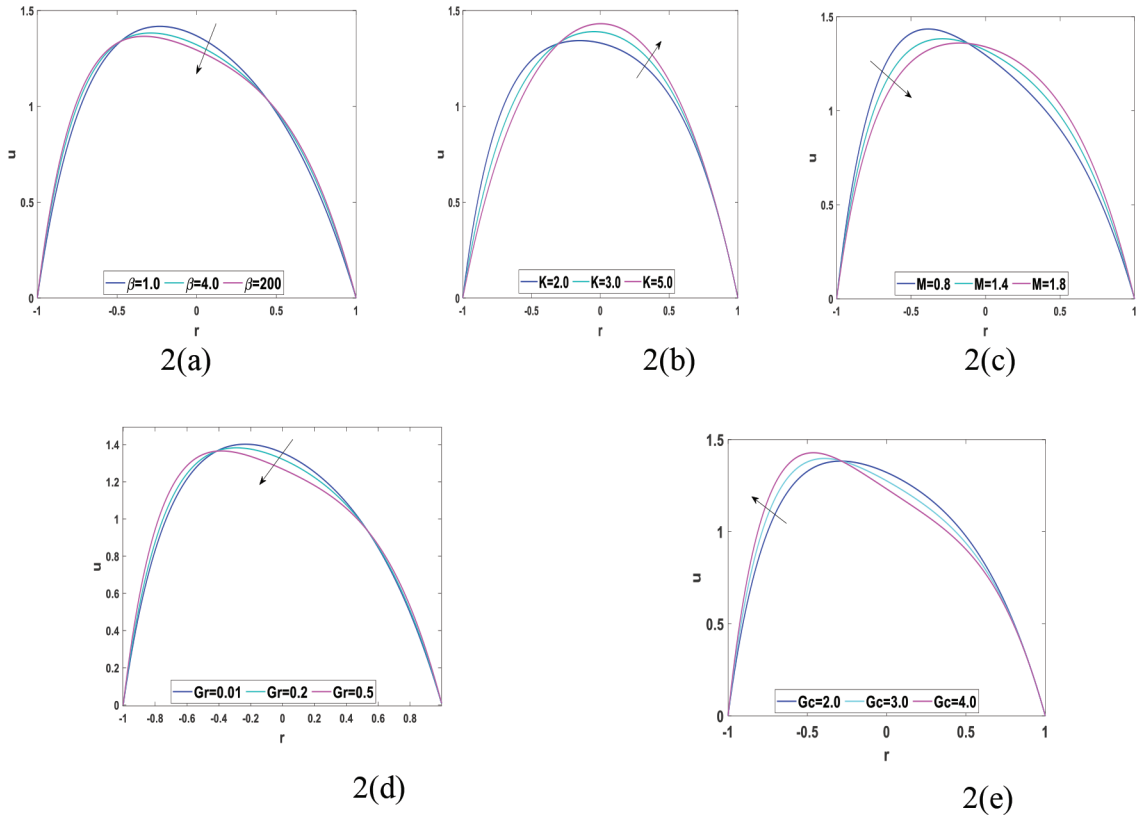


Figure 2. Velocity profile: F=1.0, β=4.0, K=2.0, M=1.4, Gr=0.2, Gc=2.0, Br=2.0, Rn=0.2, Sc=0.2, Sr=2.0

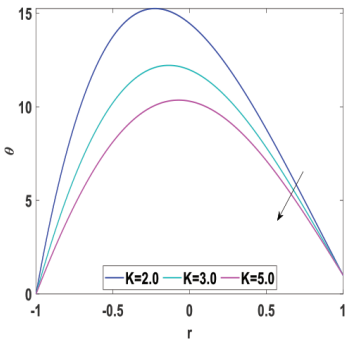
buoyancy force to viscous force, induced by temperature difference. As Gr increases buoyancy force increases there will be better mixing and redistribution of thermal energy. But we do not observe steep temperature gradient *w.r.t* Gr. Weaker buoyancy force results in less vigorous flow, leading to reduced flow velocity, as observed in Figure 2(d). Concentration Grashoff number Gc is the ratio of buoyancy force to viscous force, induced by concentration difference. Buoyancy force results in more vigorous flow, resulting in increase in velocity. This can be seen in Figure 2(e).

3.2 Temperature Profile

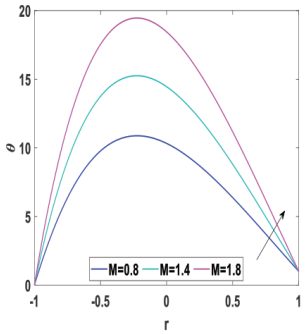
As K increases velocity of fluid flow also increases, as seen in Figure 2(b). This leads to higher viscous dissipation, and consequently energy dissipation. This decreases temperature, as seen in Figure 3(a). As M increases Lorentz force increases. This increases resistance to fluid flow, which leads to reduced mixing. Due to this there will be increase in viscous heating and hence increase in temperature, as observed in Figure 3(b). Brinkmann number Br is the ratio of heat produced by viscous dissipation to heat transported by conduction. Higher the value of Br more is the heat produced. But conduction of heat is slower, leading to temperature gradient. Hence temperature increases with large gradient. This is shown in Figure 3(c). Radiation parameter Rn is the ratio of heat produced by viscous dissipation to heat conduction. Increase in Rn increases radiative heat transfer. This increases temperature. But conduction of heat is slower, leading to temperature gradient, as we observe in Figure 3(d).

3.3 Concentration

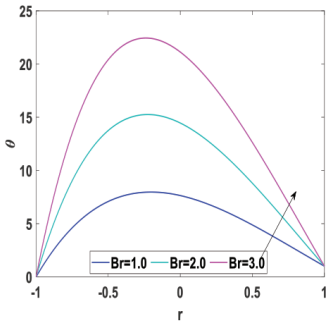
Greater K increases there is an enhanced mixing of particles, leading to decrease in concentration. Same is observed in Figure 4(a). As M increases, there is suppression of fluid flow, decreasing the mixing and dispersion of particles. Also, from Figure 3(b) we observe rise in temperature and temperature gradient.



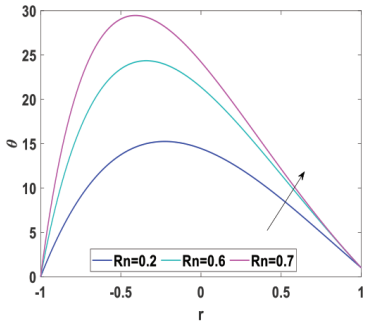
3(a)



3(b)



3(c)



3(d)

Figure 3. Temperature profile: F=1.0, β=4.0, K=2.0, M=1.4, Gr=0.2, Gc=2.0, Br=2.0, Rn=0.2, Sc=0.2, Sr=2.0

As a consequence, we see, through Figure 4(b), that there is decrease in concentration. Higher Br signify that heat is generated due to viscous dissipation, which can lead to increased fluid mixing. But conduction of heat is slow. This leads to increase in concentration, with greater gradient. Observable in Figure 4(c). Higher Rn indicate increased radiation heat transfer within the fluid. This leads to better heat transfer. This promotes better mixing and mass transport, leading to decrease in concentration. Justified by Figure 4(d). Schmidt number Sc is the ratio of momentum diffusivity to mass diffusivity. As Sc increases enhanced momentum promote dispersion of particles, leading to uniform distribution of mass. Hence, we see decreased concentration. Higher the value of Sc greater is the dispersion and reduction in accumulation. Hence there is huge concentration gradient. This is depicted in Figure 4(e). As Soret number Sr increases thermal diffusion is more than mass diffusion. Hence particles move from higher temperature region to lower temperature region, contributing to better mixing. This leads to decrease in concentration locally. This is shown in Figure 4(f).

3.4 Pressure Variation

As β increases fluid flow rate decreases. This reduces pressure gradient dp/dx, as seen in Figure 5(a). As K increases pressure gradient increases, since curvature puts forth obstacles and changes in direction of flow. This is observed in Figure 5(b). As M increases, increasing Lorentz force resists the flow. This enhances pressure gradient to overcome the magnetic forces. Justified in Figure 5(c). As both Gr and Gc increases there will be better mixing due to buoyancy force. This leads to more homogeneous distribution of velocity and temperature. Hence, we see reduction of pressure gradient. Seen in Figures 5(d) and 5(e).

3.5 Nusselt Number

Nusselt number Z is the ratio of heat transfer by convection to heat transfer by conduction. Increasing K increases fluid velocity. As seen in Figure 2(b). This promotes better mixing of fluid particles, leading to more uniform distribution of temperature. Hence there will be reduction in temperature variation. This can be observed in Figure

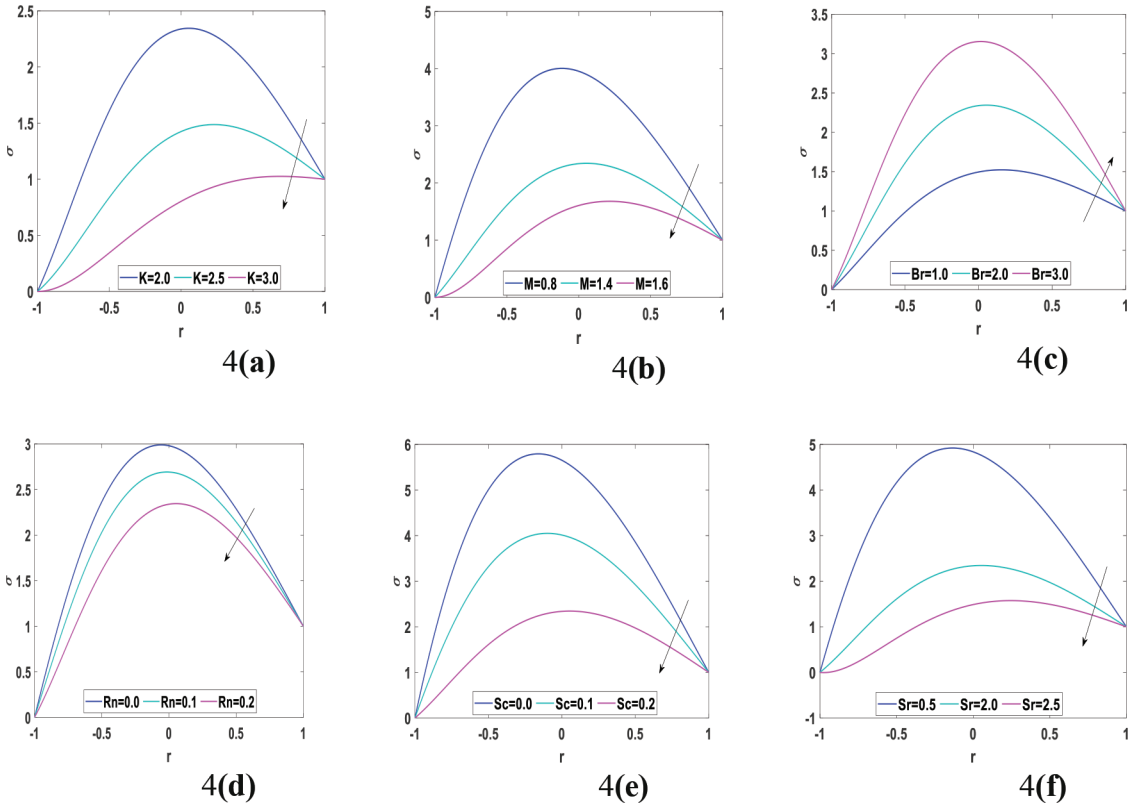


Figure 4. Concentration profile: F=1.0, β=4.0, K=2.0, M=1.4, Gr=0.2, Gc=2.0, Br=2.0, Rn=0.2, Sc=0.2, Sr=2.0

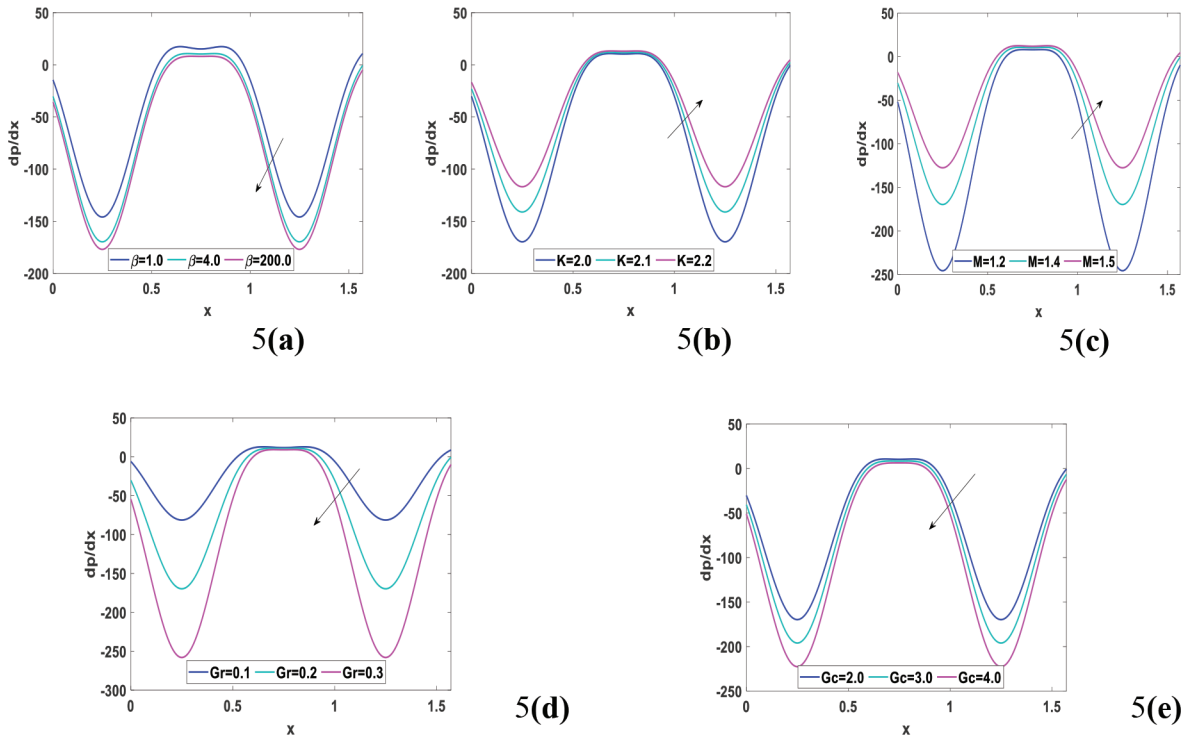


Figure 5. Pressure variation profile: F=1.0, β=4.0, K=2.0, M=1.4, Gr=0.2, Gc=2.0, Br=2.0, Rn=0.2, Sc=0.2, Sr=2.0

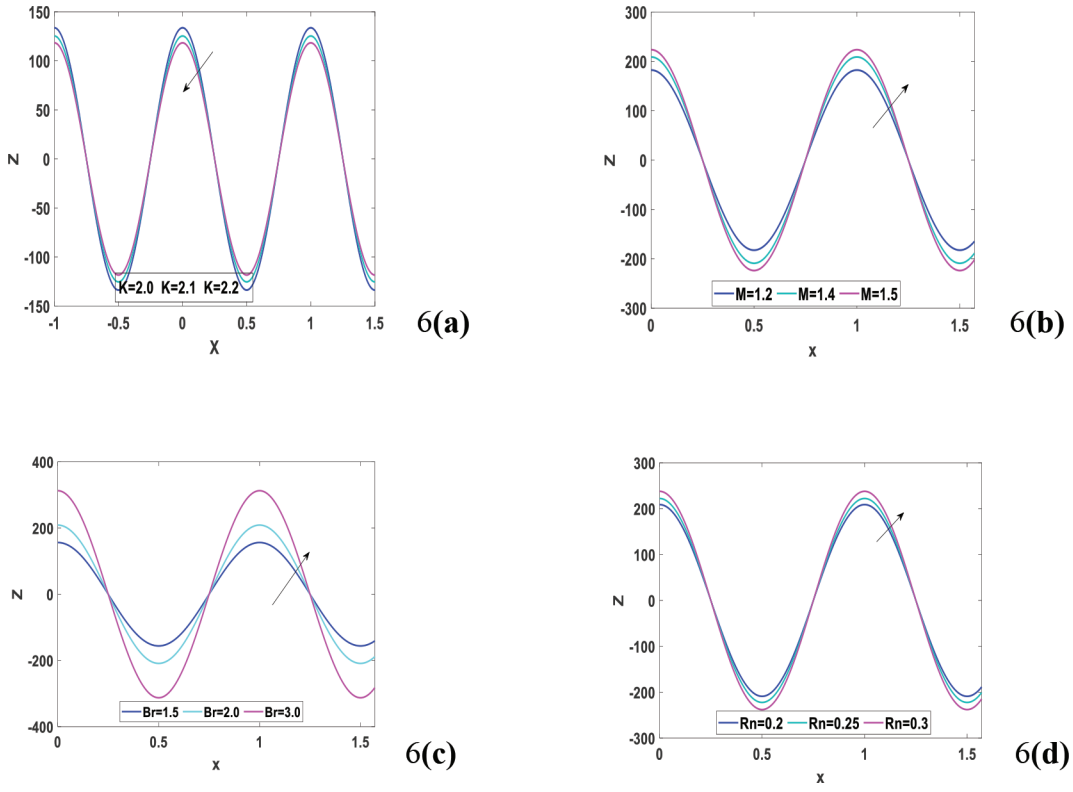


Figure 6. Nusselt number variation: F=1.0, β=4.0, K=2.0, M=1.4, Gr=0.2, Gc=2.0, Br=2.0, Rn=0.2, Sc=0.2, Sr=2.0

6(a). Increasing value of M increases Lorentz force. But induced Lorentz force enhance convective heat transfer. Hence Nusselt number increases as M increases. Figure 6(b) depicts the situation. Higher Br leads to stronger viscous forces, which promote viscous dissipation. This leads to rise in temperature. At the same time there is reduction in conduction, leading to higher temperature gradient. Hence as M increases Nusselt number also increases, as in Figure 6(c). Increasing Rn leads to stronger radiative heat transfer within the fluid. This mechanism supplements convective heat transfer, leading to increased Nusselt number, as seen in Figure 6(d).

3.6 Sherwood Number

The **Sherwood number** Sh is the ratio of the convective mass transfer to the mass diffusivity. As β increases yield stress also increases. Hence viscosity increases, hindering

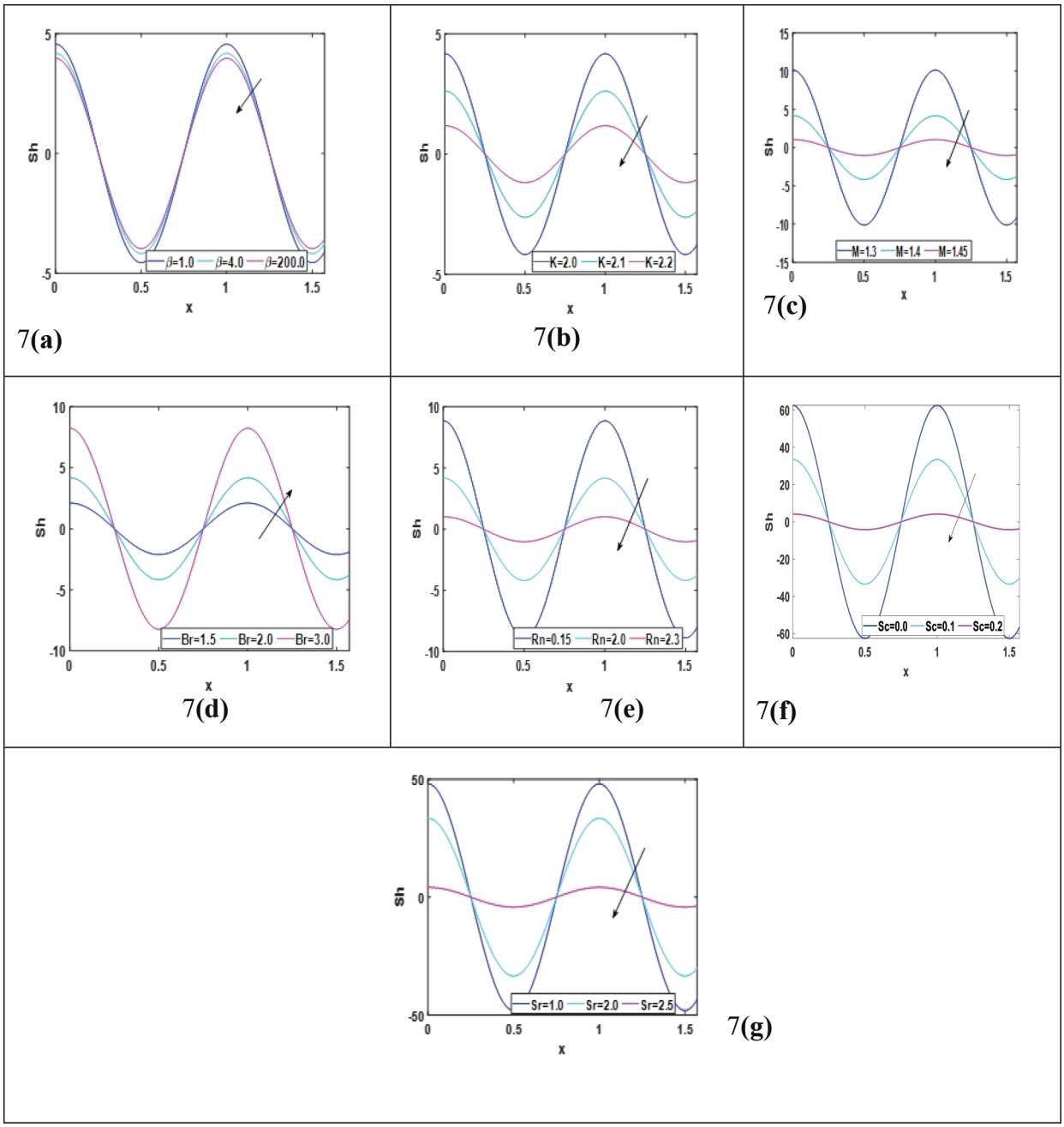


Figure 7. Sherwood number variation: F=1.0, β=4.0, K=2.0, M=1.4, Gr=0.2, Gc=2.0, Br=2.0, Rn=0.2, Sc=0.2, Sr=2.0

the flow. This leads to reduction of convective mass transfer. So, Sherwood number decreases as β increases, as shown in Figure 7(a). Increasing K increase velocity increases, as seen in Figure 2(b). This reduces residue time for the fluid particles, which reduces rate of mass transfer. Hence Sh decreases, as K increases. This is depicted in Figure 7(b). Increasing M induce stronger electromagnetic forces, which can lead to a reduction in flow velocity due to increased flow resistance. The lower flow velocities result in decreased convective mass transfer rate, contributing to a decrease in the Sherwood number. Hence Sh decreases as M increases, which is shown in Figure 7(c). Higher Br can facilitate more efficient heat transport within the fluid by promoting fluid mixing. This increased heat transport enhances the rate of mass transfer by maintaining higher temperature gradients within the fluid, resulting in improved convective mass transfer and a higher Sherwood number. Hence Sh increases as Br increases, which is shown in Figure 7(d). Higher Rn can lead to stronger radiation heat transfer within the fluid. This results in increase in temperature and concentration decrease within the fluid. This leads to faster mixing, reducing concentration gradient. Hence rate of mass transfer decreases, leading to decrease in Sh. This is observable in Figure 7(e). Higher Sr indicate a stronger influence of thermal diffusion. This can lead to increased thermal mixing within the fluid, resulting in a more uniform temperature distribution. However, uniform temperature distribution tends to decrease the temperature gradients, which are essential for driving convective mass transfer, leading to a lower Sh. Hence as Sr increases Sh decreases, as shown in Figure 7(g). Increasing Sc implies stronger momentum transfer. This can lead to increase fluid flow, reducing mass transfer. This leads to decrease in Sh. Hence as Sc increases Sh decreases. That can be observed in Figure 7(f).

4.0 Concluding Remarks

On the basis of the above assumptions and values of various parameters we come to certain conclusions. Velocity, temperature, concentration, and pressure variation profile decrease with increasing β because of its shear thinning character. Due to increasing K, velocity and pressure variation increases due to centrifugal force. Wherein temperature, concentration, Nusselt number and Sherwood number decrease due to better mixing of particles. As M increases velocity, concentration and Sherwood number decreases due to the effect of retarding force. But due to viscous heating, temperature, pressure variation and Nusselt number increase. Due to increasing Br temperature, concentration, Nusselt and Sherwood number increase due to rise viscous dissipation. As Rn increases, due to better heat transfer, temperature and Nusselt number increase, whereas concentration and Sherwood number decreases.

5.0 References

1. Ali N, Sajid M, Javed T, Abbas Z. Heat transfer analysis of peristaltic flow in a curved channel. Int J Heat Mass Transf. 2010; 53(15-16):3319-25. https://doi.org/10.1016/j.ijheatmasstransfer.2010.02.036
2. Abd-Alla AM, Abo-Dahab SM, Thabet EN, Abdelhafez MA. Heat and mass transfer for MHD peristaltic flow in a micropolar nanofluid: Mathematical model with thermophysical features. Sci Rep. 2022; 12. https://doi.org/10.1038/s41598-022-26057-6
3. Kothandapani M, Prakash J. Effect of radiation and magnetic field on peristaltic transport of nanofluids through a porous space in a tapered asymmetric channel. J Magn Magn Mater. 2015; 378:152-63. https://doi.org/10.1016/j.jmmm.2014.11.031
4. Akbar NS, Nadeem S, Khan ZH. Numerical simulation of peristaltic flow of a carreau nanofluid in an asymmetric channel. Alex Eng J. 2014; 53(1):191-7. https://doi.org/10.1016/j.aej.2013.10.003
5. Bhargava IR, Singh S. Numerical simulation of unsteady MHD flow and heat transfer of a second grade fluid with viscous dissipation and joule heating using meshfree approach. IJMEMS. 2012; 6(6):660-6.
6. Venkateswarlua B, Narayana PVS, Tarakaramub N. Melting and viscous dissipation effects on MHD flow over a moving surface with constant heat source. Trans A Razmadze Math Inst. 2018; 172(3 Part B):619-30. https://doi.org/10.1016/j.trmi.2018.03.007
7. Makindea OD, Reddy MG. MHD peristaltic slip flow of casson fluid and heat transfer in channel filled with a porous medium. Sci Iran Trans B. 2019; 26(4):2342-55. https://doi.org/10.24200/sci.2018.20319
8. Rashidi M, yang Z, Bhatti M, Abbas M. Heat and mass transfer analysis on MHD blood flow of casson fluid model due to peristaltic wave. Therm Sci. 2018; 22(6 Part A):2439-48. https://doi.org/10.2298/tsci160102287r
9. Asha SK, Sunitha G. Effect of joule heating and MHD on peristaltic blood flow of Eyring-Powell nano fluid in a non-uniform channel. J Taibah Uni Sci. 2019; 13(1):155-68. https://doi.org/10.1080/16583655.2018.1549530

10. Abbasi FM, Shehzad SA. Heat transfer analysis for EMHD peristalsis of ionic-nano fluids via curved channel with joule dissipation and Hall effect. J Biolog Phys. 2021; 47:455-76. https://doi.org/10.1007/s10867-021-09582-9
11. Abbasi FM, Shehzad SA. Impact of curvature-dependent channel walls on peristaltic flow of Newtonian fluid through a curved channel with heat transfer. Arab J Sci Eng. 2020; 45:9037-44. https://doi.org/10.1007/s13369-020-04653-w
12. Hu Z, Azmi SM, Ghulam R, Paul WJG, Dongsheng W. Nanoparticle-assisted water-flooding in Berea sandstones. Energy Fuels. 2016; 30(4):2791-804. https://doi.org/10.1021/acs.energyfuels.6b00051
13. Zhang T, Davidson D, Bryant S, Huh C. Nanoparticle-stabilized emulsions for applications in enhanced oil recovery. Proc - SPE Symp Improv Oil Recovery. 2010. https://doi.org/10.2523/129885-ms
14. Suleimanov BA, Ismailov FS, Veliyev EF. Nanofluid for enhanced oil recovery. J Pet Sci Eng. 2011; 78(2):431-7. https://doi.org/10.1016/j.petrol.2011.06.014
15. Moghadam TF, Azizian S. Effect of ZnO nanoparticles on the interfacial behavior of anionic surfactant at liquid or liquid interfaces. Colloids Surf A: Physicochem Eng. 2014; 457:333-9. https://doi.org/10.1016/j.colsurfa.2014.06.009
16. Adil M, Lee K, Zaid MH, Latiff NRA, Alnarabiji MS. Experimental study on electromagnetic-assisted ZnO nanofluid flooding for enhanced oil recovery (EOR). PloS one. 2018; 13(2):e0193518. https://doi.org/10.1371/journal.pone.0193518
17. Asha SK, Kallolikar N. Thermal analysis for peristaltic flow of nanofluid under the influence of porous medium and double diffusion in a non-uniform channel using sumudu transformation method. Annals of Pure and Applied Mathematics. 2021; 23(2):73-91. https://doi.org/10.22457/apam.v23n2a05817
18. Murugesan T, Kumar MD. Viscous dissipation and Joule heating effects on MHD flow of a Thermo-Solutal stratified nanofluid over an exponentially stretching sheet with radiation and heat generation or absorption. Int World Sci J. 2019; 129:193-210.